Degradation and bioconversion of complex municipal solid waste streams into human biotherapeutics and biopolymers

Guadalupe Alvarez-Gonzalez[†^], Micaela Chacón[†^], Adokiye Berepiki[†], Karl Fisher[†], Neil Dixon[†*]

[†]Manchester Institute of Biotechnology (MIB), Department of Chemistry, University of Manchester, Manchester, M1 7DN, UK

[^]These authors contributed equally

*Corresponding author

Abstract

Linear consumption models in combination with the poor waste management results in negative impact upon the climate and environment. Here we show an advanced biorefinery concept to produce biopolymers and recombinant therapeutic proteins from municipal solid waste. Careful selection and metabolic engineering of *Pseudomonas putida* was employed to permit efficient co-utilisation of complex, heterogenous substrate compositions derived from the most abundant municipal solid waste fractions. Enzymatic pre-treatment of the feedstock was performed, which afforded sufficient carbon for growth and bio-production of value-added products. Unlike current waste processing methods and supply of feedstocks for bio-based manufacturing, this biorefinery concept re-directs the carbon away from direct emissions and creates a land-use negative feedstock ideal for advanced biomanufacturing. We envisage this demonstration will lead to the creation of circular consumption solutions for waste and bio-production of a range of chemicals and materials in future resource finite scenarios.

Main

Global supply chains are dominated by linear, carbon positive, economic models; extract, use, dispose, which creates unsustainable systems reliant on finite geological reserves. Growing awareness of the damaging impact of this model upon the climate has spurred urgent action by the international community to find solutions to mitigate greenhouse gas emissions[1–6]. Biotechnology provides opportunities to shift from a linear to a more circular bio-based economic model. Towards this, the concept of biorefinery emerged as an analogue to the petroleum-based refinery industry, where fuel, power, chemicals and materials can be derived from renewable biomass[7]. While first and second generation biomass feedstocks provide carbon circularity, there are concerns around the diversion and expansion of arable land use towards agro-industrial production[8]. In light of projected population growth and rising sea levels, land use will become more crucial, and dedicated allocation to feedstocks for biorefineries less sustainable[9,10]. Instead, focus is now shifting towards the use of organic process residuals and wastes from the agricultural, forestry, paper and pulp and food industries as biorefinery inputs[11–14]. Whilst this supports a more circular bioeconomy future[6,15], to date, the use of such waste-to-feedstock symbioses has been limited to industrial pre-consumer waste streams with limited heterogeneity.

Municipal solid waste (MSW) represents a highly heterogeneous mix of biogenic and non-biogenic household, commercial and industrial waste collected by a local municipality. Currently, global MSW generation is estimated to exceed 2 billion tonnes per year and is predicted to further increase to 3.4 billion tonnes per year by 2050[16,17]. The composition of MSW can vary considerably depending on climate, season, culture, and income level, reflecting different global patterns of consumption. However, on average, MSW in low-income countries is comprised of more than 50% green and food waste, while recyclables, metal, glass, paper and plastic are dominant in high-income countries[17,18]. Economic status is also a dominant factor for waste management strategy, up to 96% of waste is sent to dumps and landfill in low-income countries, compared to 41% in high-income countries – together contributing 1.6 billion tonnes of carbon dioxide emission equivalents per year[17,19]. Current strategies for MSW valorisation depend on the nature of the waste. Biogenic fractions can be composted or fed into anaerobic digestion (AD) where the outputs are fertilizer and biogas, while non-biogenic fractions can undergo incineration or pyrolysis which generate energy. These valorisation strategies however require strict constraints on waste-feedstock composition, e.g., moisture and sugar content, carbon to nitrogen ratio, and heating value[19,20]. In addition, the end-products from each of the above are fixed, therefore expanding the variety of bio-based building blocks, chemicals and materials via microbial production would offer more versatile opportunities for waste valorisation[21,22]. MSW also has many positives as a potential feedstock for a distributed manufacturing scenario; its global distribution and links to population density reduce the need for additional transportation cost and impact.

Depending on the region, between 60-85% of MSW is carbonaceous, made up of food waste, garden waste, paper and board, plastic, textile, leather and rubber[18]. A wealth of studies have been performed to develop enzymes for the degradation of the individual polymers and macromolecules that make up these waste fractions[23–26]. Once broken down to their monomeric units, these can be fed into the metabolism of microbial cell factories to produce value-added products[27,28]. However, despite the body of work on the valorisation of individual waste streams, little has been done towards complex mixed waste stream valorisation. An inherent challenge of using an MSW feedstock for microbial-based production is the efficient utilisation of the complex mixture of organic carbon substrates released from the enzymatic hydrolysis[29]. Most microbes consume mixed substrates selectively due to incompatible metabolism, or sequentially with long diauxic lag times between preferred substrates, prolonging microbial cultivation time and reducing the efficiency of carbon conversion – essential aspects of a cost-effective production platform[30]. In the context of MSW, its compositional heterogeneity and periodical variability can result in huge variation in the ratio and range of carbon substrates. Therefore, microbial host selection must be carefully considered to ensure the host is genetically tractable, displays versatile metabolic capabilities, and can be manipulated to permit growth on complex, dynamic, heterogenous substrate compositions.

Pseudomonas putida is a soil dwelling bacterium that displays high solvent tolerance and is considered to be a robust host for bioproduction and bioremediation applications[31,32]. It possesses remarkably flexible non-archetypal metabolism that can accept divergent carbon substrates with no overflow metabolism and rapid shift/adaptation to nutrient availability without a long lag-phase[33]. Previous reports have shown that engineered strains of *P. putida* are capable of substrate co-utilisation, of up to five substrates, sugars, aromatics, and acids, derived from pre-treated lignocellulose[34], and more recently, substrates derived from metal-catalysed autoxidation of mixed plastics[35]. This catabolic activity paired with facile genetic tractability make *P. putida* an ideal host for heterogeneous feedstocks.

In this work, we demonstrate tandem enzymatic-whole cell valorisation of five key MSW fractions using a tailored enzyme cocktail and a strain of *P. putida* engineered to co-utilise the common monomeric substrates derived from MSW hydrolysis: glucose, xylose, ferulic acid, coumaric acid, C_{12}-C_{18} fatty acids, glycerol, terephthalic acid (TPA), ethylene glycol (EG), and lactic acid (**Fig. 1**). We demonstrate the flexibility of this platform to accept divergent waste compositions as an input, and to produce distinct value-added products as an output. This proof-of-concept work illustrates the versatility of microbial based biorefineries in the valorisation of MSW, is a first step towards diversifying the valorisation opportunities from MSW, and expands the biorefinery concept to other, land-use negative, waste-feedstocks.

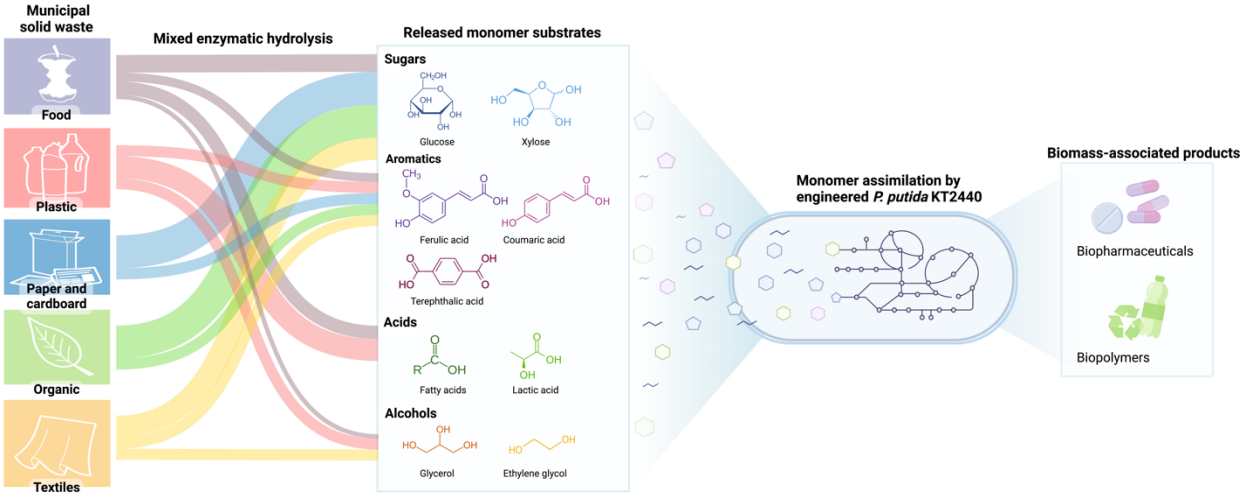

Figure 1. Concept process for the degradation and valorisation of municipal solid waste streams into valuable products. The most common carbon-based municipal solid waste fractions are enzymatically hydrolysed in a one-pot process, resulting in the release of different ratios of monomeric substrates. These monomers are subsequently co-utilised as the sole carbon and energy sources by an engineered *Pseudomonas putida* capable of synthesising biomass-associated products, including biotherapeutics and biopolymers.

Results

Ethylene glycol enhances recombinant therapeutic protein production in engineered *P. putida* KT2440 grown on terephthalic acid

As a first step towards achieving the biological valorisation of MSW to valuable products (**Fig. 1**), we sought to engineer a robust microbial strain capable of co-assimilating the main monomeric substrates making up the selected waste fractions. First, we aimed to engineer *Pseudomonas putida* KT2440 to assimilate TPA and EG, the monomers of polyethylene terephthalate (PET) plastic. In order to achieve this, we developed a genetic construct expressing a TPA catabolic operon (*tphA2$_{II}$A3$_{II}$B$_{II}$A1$_{II}$*) from *Comamonas* sp. E6[36,37] and a TPA transporter, *tphK,* from *P. mandelli* JR1. In anticipation of the varying TPA availability from the distinct waste compositions and to avoid the metabolic burden imposed from overexpressing this pathway, we employed a dynamic feedback loop to fine-tune the expression of the *tph* operon according to available TPA concentrations. Therefore, we placed the *tph* catabolic operon and the *tphK* transporter under the control of an optimised protocatechuate (PCA)-inducible module that we had previously developed[38] (**Fig. 2a**). The resulting p131CB10-tphKAB plasmid was introduced into *P. putida,* generating strain **tphKAB**. This strain could utilise 10 mM of TPA as a sole carbon and energy source within 24 h (**Fig. 2b**, **Fig. S1a**) at a growth rate of 0.227 ± 0.021 h^{-1}, reaching a maximum biomass yield of $Y_{X/S}$ of 0.33 g_{CDW} g_{TPA}^{-1}.

We next set out to further modify this strain to assimilate EG. *P. putida* KT2440 can only inefficiently utilise EG for biomass accumulation when it is present in high concentrations, partly due to complex regulatory mechanisms surrounding C_2 metabolic pathways[39,40]. One such mechanism involves repression of the glyoxylate carboligase (*gcl*) pathway, by GclR. After the conversion of ethylene glycol to glyoxylate by the glycolate oxidase (*glcDEF*) operon, *gcl* can allow EG assimilation into biomass via glycerate metabolism[41] (**Fig. 2d**). Overexpressing both operons and/or deleting *gclR* has therefore been shown to significantly improve ethylene glycol metabolism as a sole carbon and energy source[37,41]. Here we employed a similar approach whereby both promoters driving expression of the *gcl* and *glcDEF* operons were exchanged by the strong constitutive P_{tac} promoter in the tphKAB strain. The resulting strain **tphKAB-EG12** (*P. putida* KT2440 p13CB10:*tphKA2$_{II}$A3$_{II}$B$_{II}$A1$_{II}$* Ptac::*glcDEFG* Ptac::*gcl*) could utilise 10 mM of both TPA and/or EG as the sole carbon and energy source (**Fig. S1b-c**). Moreover, growth in the presence of both TPA and EG was additive, reflected by an increased cell density by almost 30% over that achieved on TPA alone, (OD_{600} of 1.9 and 1.35, respectively), suggesting both monomers are simultaneously funnelled into biomass (**Fig. 2**). Interestingly, when grown on both substrates, the parental tphKAB strain could also fully consume EG, albeit without it leading to biomass accumulation (**Fig. 2b**). Though both the tphKAB and tphKAB-EG12 strains exhibited similar growth rates when co-fed TPA and EG (0.227 ± 0.021 h^{-1} and 0.250 ± 0.012 h^{-1}, respectively), tphKAB could more efficiently uptake both substrates,

while tphKAB-EG was able to better assimilate them into biomass, reflected by its lower substrate uptake rates and higher biomass yield (**Fig. 2c**).

To establish which genetic scenario offered the optimal flux configuration for EG in the proposed process, we compared the ability of both strains to produce a panel of recombinant therapeutic proteins (RTP) when grown on TPA and EG as sole carbon and energy sources. These included several tagged long-acting human insulin analogues (INS1, INS2, INS3)[42], human interferon α2a (IFNα2a), and a synthetic HEL4 nanobody (Nb1). Both strains were able to produce all recombinant proteins when grown on TPA and EG as the sole carbon and energy sources (**Fig. 2b**). Despite lower biomass accumulation, recombinant protein production titres were on average 7-fold higher in the tphKAB strain, as observed by western blot densitometry (**Fig. 2**). This increase was only observed with EG co-feeding in the tphKAB strain, as yields obtained with this strain grown solely on TPA were similar to those from tphKAB-EG (**Fig. S1d**). Therefore, due to the protein yield enhancement observed, we utilised tphKAB as the base strain for all further engineering, and we selected IFNα2a as the model RTP example moving forward.

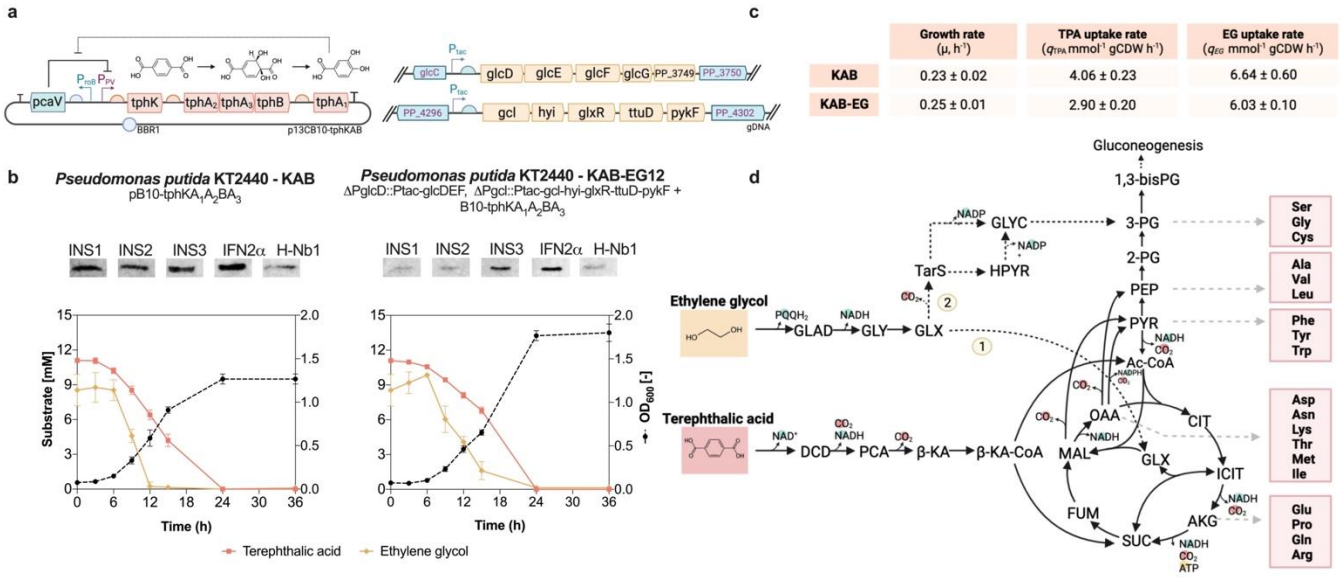

Figure 2. Engineered metabolism and therapeutic protein production from TPA and EG by engineered *P. putida*. (**a**) Schematic of catabolic modules enabling EG (top) and TPA (bottom) metabolism in *P. putida.* The *tph* operon ($tphA2_{II}A3_{II}B_{II}A1_{II}$) from *Comamonas* sp. E6 and the *tphK* transporter from *P. mandelii* are placed under the control of a PCA-sensing module[38]. The *glcDEF* (P_{tac}:*glcDEFG:PP_3750*) and gcl (*gcl*:*hyi*:*glxR*:*ttuD*:*pykF*) operons are overexpressed by downstream introduction of a P_{tac} constitutive promoter. (**b**) Growth, substrate utilisation and production of a panel of long-acting human insulin analogues (INS1, INS2, INS3), human interferon α2a (IFNα2a), and a synthetic HEL4 nanobody (Nb1), from strains tphKAB (harbouring TPA metabolism only) and tphKAB-EG (harbouring TPA and EG metabolism) grown in shake flasks

containing 10mM of both TPA and EG. Error bars indicate the SD between triplicates. (**c**) Growth rates (μ) and substrate uptake rates (q_{SUB}) calculated from flask growth and consumption curves of both strains. (**d**) Metabolic pathways for the assimilation of TPA and EG in the engineered *P. putida* KT2440 strains. In the tphKAB strain, EG is natively funnelled into the glyoxylate shunt (1), while in the tphKAB-EG strain, EG is metabolized to biomass directly from 3-PG (2).

Engineered *P. putida* KT2440 co-utilises a mixture of different substrates derived from municipal solid waste feedstocks

We next sought to explore the growth and co-utilization of the substrates derived from the selected MSW fractions in the tphKAB strain. *P. putida* KT2440 can natively metabolize the remaining selected aromatic substrates, acids, alcohols, and glucose. However, we needed to further engineer tphKAB to be able to utilise xylose as a sole carbon and energy source, as it is not able to metabolize C_5 sugars. For this purpose, we integrated the D-xylose isomerase pathway from *E. coli* into the tphKAB strain. In this pathway, xylose is transported by the D-xylose:H^+ symporter (*xylE*) and metabolized via the D-xylose isomerase (*xylA*) and xylulokinase (*xylB*) to xylulose-5-phosphate (X5P) where it can then enter central metabolism. We additionally deleted glucose dehydrogenase (*gcd*) to avoid conversion of xylose to the dead-end product xylonate[43]. This enzyme is also involved in the periplasmic conversion of glucose to gluconate during glucose metabolism. As expected, the final strain tphKAB-XylABE was able to grow on xylose as a sole carbon and energy source (**Fig. S2**). The deletion of *gcd* resulted in a slight detrimental impact on the growth and uptake rate of tphKAB-XylABE on glucose alone, partly due to ATP-costly glucose uptake via an ABC transporter (GtsABCD)[43], although there was no difference in the total biomass achieved (both OD_{600} = 1.7, **Fig. S2b**).

The final engineered strain tphKAB-XylABE was thus able to efficiently assimilate terephthalic acid, ethylene glycol, lactic acid, glucose, xylose, ferulic acid, *p*-coumaric acid, glycerol, and fatty acids when individually provided as the sole carbon and energy source (**Fig. S3**). To gain additional insight into the carbon conversion from each substrate, we constrained a modified genome-scale metabolic model (GEM) of *P. putida* KT2440 with the experimentally obtained metabolic data and performed flux balance analysis (FBA). FBA was able to accurately predict a growth rate for each individual substrate (R^2 = 0.9524, **Fig. S4**), and so we used this method to obtain a prediction of the CO_2 production rate for each substrate. High yields of biomass per substrate were obtained in descending order with fatty acids, lactic acid, and glycerol (1.34 g_{CDW} g^{-1}, 0.69 g_{CDW} g^{-1} and 0.58 g_{CDW} g^{-1}, respectively). When using these preferential substrates alone, *P. putida* funnelled more than 60% of the substrate's C-mol content into biomass rather than CO_2 (**Fig. 3a**). The lowest biomass yield was obtained with terephthalic acid and ethylene glycol, partly due to ethylene glycol serving as an energy co-substrate only (0.26 g_{CDW} g_{TPA}^{-1}), with a loss of 74% of the total carbon to CO_2 (**Fig. 3a**). The remaining substrates afforded moderate biomass yields, similar to that of glucose (0.43 g_{CDW} g_{GLU}^{-1},

0.48 g_{CDW} g_{FA}^{-1}, and 0.44 g_{CDW} g_{CA}^{-1}), with 33 to 53% of their C-mol content channelled to biomass (**Fig. 3a**). In terms of growth rate, fatty acids and lactic acid provided the fastest growth, at 0.466 ± 0.05 h^{-1} and 0.489 ± 0.006 h^{-1} respectively. Moderate growth rates were observed for glucose, terephthalic acid and ethylene glycol, coumaric acid and glycerol, while growth on ferulic acid and xylose were slowest (0.102 ± 0.003 h^{-1} and 0.04 ± 0.002 h^{-1}, respectively).

After validating growth on each individual substrate, we next evaluated growth from co-utilisation of all nine monomers. We performed flask growth assays with tphKAB-XylABE in minimal M9 medium containing equimolar (10 mM) concentrations of all nine carbon sources (**Fig. 3b**). The equimolar combination of all substrates afforded a high maximum OD_{600} of 7.4 at a growth rate of 0.275 ± 0.016 h^{-1}, reaching a final combined biomass yield of 0.47 g_{CDW} g_{SUB}^{-1}. We noticed three distinct growth and consumption phases corresponding to early- (12-23 h), mid- (23-30 h) and late- exponential (30-39h) before reaching stationary phase (39-72 h). Lactic acid was preferentially consumed during the early exponential phase, along with a small amount of glucose, fatty acid, and aromatics (**Fig. 3b**). Lactic acid contributed roughly the same amount to biomass accumulation as when present as a sole carbon source, albeit at a slower uptake rate (10.5 ± 1.2 vs 2.3 ± 0.2 mmol g_{CDW}^{-1} h^{-1}). During this early period, modelling predicts a TCA cycle operating via the glyoxylate shunt, predominantly driven by lactic acid metabolism and from minor additional acetyl-CoA and intermediate organic acid influx from β-oxidation and aromatic degradation, respectively[44] (**Fig. 3c & Fig. S5**). Here, central metabolism operates under a gluconeogenic configuration, driving flux towards 3-phosphoglycerate (3-PG). During mid- and late-exponential phase, the remaining carbon sources were utilised simultaneously (**Fig. 3b & Fig. S5**), with TPA, glycerol, glucose and fatty acids being depleted by 48 hours. This period afforded the principal growth, reaching a maximum OD_{600} of 7.4. Flux predictions during mid-exponential phase, indicate all substrates were being co-utilised, although gluconeogenic substrates were used preferentially to glycolytic ones, resulting in especially strong flux through TCA via glyoxylate shunt reactions. During this phase, central metabolism was still operating under a gluconeogenic configuration (**Fig. 3c**). However, flux demands in the upper Embden-Meyerhof-Parnas (EMP), pentose-phosphate (PP) and Entner–Doudoroff (ED) pathways were seemingly still satisfied, suggesting that glycerol and sugar-derived carbon was compartmentalized within these pathways[45]. At late exponential phase however, central ED shifts to a glycolytic directionality, likely due to the later (non-preferred) onset of xylose consumption (**Fig. 3c**). Because of the increased flux through these pathways, xylose was assimilated more rapidly in mixed substrate feed than when provided alone. Here it was completely depleted by 57 h, as opposed to the partial consumption observed after 120 h when present as the sole substrate (**Fig. 3c & Fig. S3**). We note that no further cell biomass accumulated beyond 39 h, even though substrates capable of contributing to growth remained (including 6.8 mM of ferulic acid and 1.86 mM of coumaric acid). This is explained by the observation that although FA and CA were partially depleted by mid-exponential phase, they had not completely journeyed through the lower aromatic catabolic pathway, and we observed a build-

up of the respective pathway intermediates vanillic acid (VA) and 4-hydroxybenzoic acid (4HBA) (**Fig. S6)**. Only after TPA had been completely depleted did 4HBA and VA consumption begin, being completely depleted by 57 h and 72 h, respectively. No significant growth increase was associated with the depletion of these intermediates, as rather they were used along with the remaining ethylene glycol to meet cell maintenance and energy requirements.

These results demonstrate how when using complex mixed substrates, *P. putida* can quickly and dynamically change the configuration of its central and peripheral metabolic pathways in response to changing carbon and energy availability. This trait is especially pertinent in the context of changing substrate ratios and concentrations from varying waste compositions. To further illustrate this, we explored the growth of the tphKAB-XylABE strain on a variety of possible combinations of the nine representative monomers. We employed a design of experiments (DoE) approach to help construct a set of treatments that would explore the full combinatorial space of a range of concentrations for each substrate (**Table S6**). Each substrate was provided in the respective treatment at either 0, 25 or 50 mM, except for ferulic and coumaric acid which were supplied at 0, 5 or 10 mM and fatty acids at 0, 12.5 or 25 mM, and grown in minimal media for 72 h. The final set of 25 conditions tested allowed us to investigate the vast number of possible scenarios at which each substrate could be found in process relevant conditions. Robust biomass yields from the combined substrates were obtained consistently across all conditions after 72h, ranging from $0.21 g_{CDW}\ g_{SUB}^{-1}$ to $0.61 g_{CDW}\ g_{SUB}^{-1}$. When accounting for the percentage of C-mmol that each substrate contributes to biomass, calculated from the individual growth experiments, we observed a correlation between the amount of calculated carbon input ($C\text{-}mmol^{IN}$) contributing to biomass from each substrate and the final biomass obtained ($C\text{-}mmol^{OUT}$) across the 25 conditions ($R^2 = 0.788$, p-value < 0.001) (**Fig. 3e**). This reiterates the fact that, regardless of the amount and concentration of each available substrate, the engineered *P. putida* strain tphKAB-XylABE can efficiently and consistently convert the available carbon into biomass.

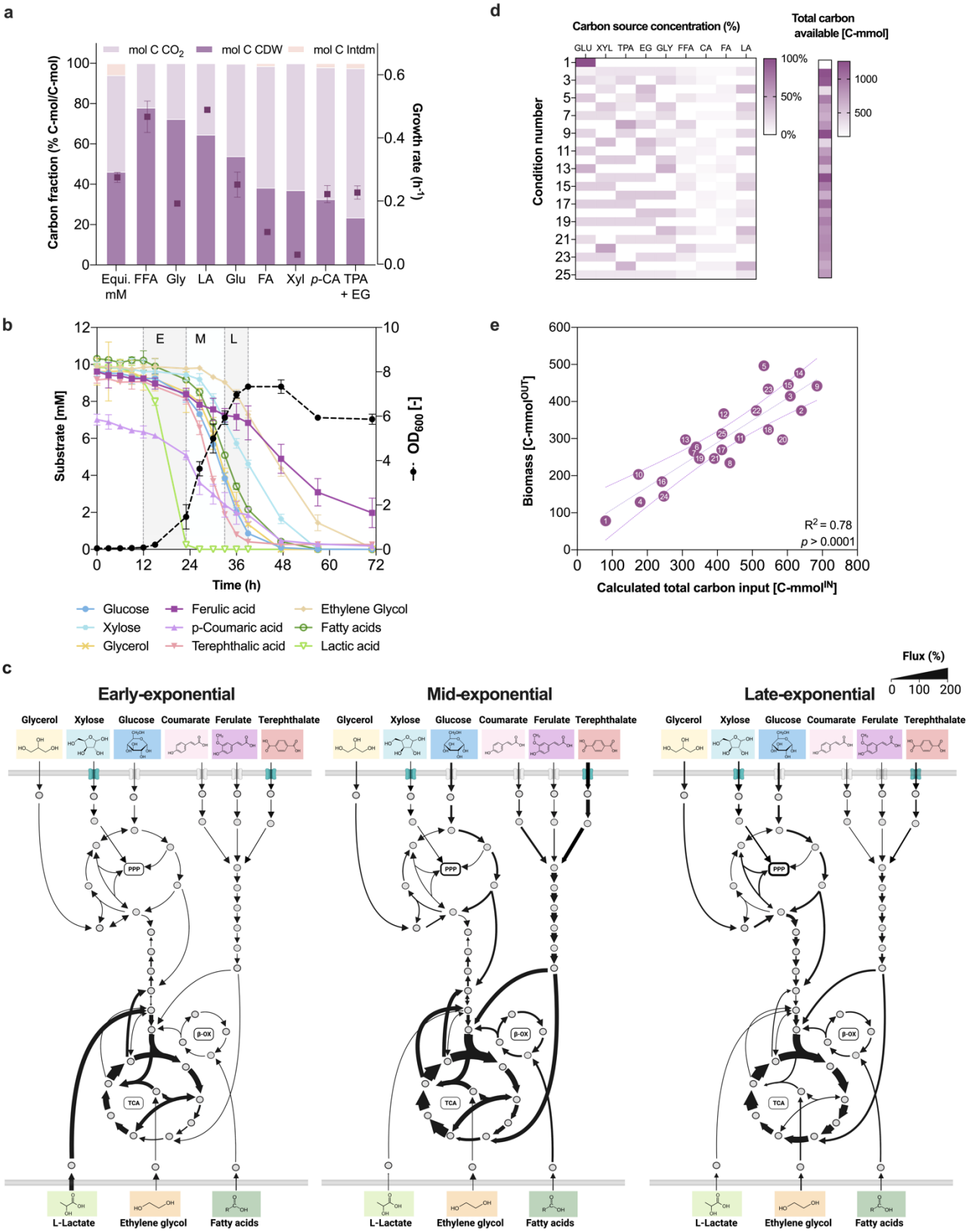

Figure 3. Engineered *P. putida* KT2440 efficiently assimilates mixtures of the nine major substrates in MSW. (**a**) Growth rates and carbon balance for flask cultivations with individual substrates. Shown are all carbon-containing substrates measured at the end of exponential phase for each monomer, where the carbon fraction represents their relative abundance to the overall input of carbon in C-mol. The amount of CO_2 produced was calculated from FBA-predicted CO_2 production rates over the whole growth period. (**b**) Flask cell cultivation profile of tphKAB-XylABE in M9 medium containing equimolar (10 mM) amounts of the

nine monomeric substrates (1.74 g L-1 glucose, 1.49 g L-1 xylose, 1.86 g L-1 ferulic acid, 1.45 g L-1 p-coumaric acid, 0.89 g L-1 lactic acid, 1.93 g L-1 terephthalic acid, 0.61 g L-1 ethylene glycol, 0.88 g L-1 glycerol and 2.47 g L-1 fatty acid). (**c**) Predicted flux distributions for the assimilation of the nine monomers in the equimolar cultivation during early, mid- and late-exponential phase. (**d**) Layout of the 25 selected treatments containing different concentrations of each substrate as proposed by design of experiments, and the total carbon available from these substrates in C-mol. (**e**) Correlation between the achieved biomass in C-mmol and the calculated total input of biomass-producing carbon. OD_{600} represents the optical density measured at 600 nm. All data are means ± SDs of N = 3 biological triplicates.

Enzymatic hydrolysis of municipal solid waste derived feedstock affords sufficient carbon to support growth of engineered *P. putida*

Investigation into the enzymatic pre-treatment of MSW began by selecting an assortment of commercial and post-consumer materials representative of the five selected MSW fractions that would be amenable to enzymatic hydrolysis (**Table S7**). For plastic waste, we selected an amorphous PET film and poly lactic acid (PLA) beads. Post-consumer municipal paper pulp was used to directly exemplify the paper and cardboard fraction. Wheat straw served as a lignocellulosic example of organic waste. For food waste, we utilised palm oil, corn cob and a mixture of micronized barley, apple, and beetroot. Finally, we obtained a cotton-polyester blended fabric to represent textile waste. As a result of differing waste management practices, the composition of municipal waste varies greatly across geographical zones[17]. A region's GDP can serve as an accurate indicator of the different consumption practices that ultimately result in distinctive waste compositions. To demonstrate our process concept's applicability when dealing with wastes of varying composition, we replicated two waste scenarios using the selected feedstocks to represent (i) high and upper-middle income countries (high) and (ii) lower-middle- and low-income countries (low) (**Fig. 4a**). In the resulting formulations, paper and cardboard constituted the predominant fraction in the high-income representation (34%), followed by food (22%), garden (21%) and plastic (18%) waste. Low-income countries comprised predominantly of food and garden waste (38% each), with only 9% of both plastics and paper and cardboard waste. Textiles contributed only a small fraction of the waste for both high- and low-income countries (5% and 6%, respectively) (**Fig. 4a**).

To minimise complexity, cost, and time, we established common pre-treatment conditions that would support the mixed enzymatic hydrolysis of these feedstocks in one pot. The representative feedstocks were prepared to the relevant ratios for the high and low-income formulas (as illustrated in **Table S7**) at a final 25% (w/w) solid loading, and both were treated with a tailored cocktail of degradative enzymes (results for individual feedstock hydrolysis can be found in **Fig. S7- S14**). Both mixed waste hydrolyses afforded release of the selected sugar, acid, alcohol, and aromatic monomers (**Fig. 4c & Fig. S15**). The major product obtained from both high- and low-income feedstock was glucose. Concordant with the increased amount of paper and cardboard, the release of sugars was higher in the high-income mixture, even though the low-income feedstock had more

total sugar-containing feedstocks. Fatty acids were the next most abundant product in both feedstocks, with a mixture of $C_{12:0}$, $C_{14:0}$, $C_{16:0}$, $C_{18:0}$, $C_{18:1}$ and $C_{18:2}$, (all of which could be utilised for cell growth (**Fig. S16**)), and the greater release was also concordant to the higher food fraction in the low-income feedstock. The lowest yields were obtained for lactic acid, ferulic and coumaric acid. A total of 9.7 g L^{-1} and 9.0 g L^{-1} of combined products were obtained for the high and low-income feedstocks, respectively, corresponding to 0.365 and 0.405 mol of total carbon (C-mol) (**Fig. 4c**).

The resulting recovered liquor was used directly for microbial cultivation in microbioreactors (**Fig. 4d**). Engineered tphKAB-XylABE was able to grow as efficiently and rapidly on synthetic media containing the same substrate concentrations (mocks) as the real MSW hydrolysates (**Fig. 4d**). This suggests that no significant amount of additional metabolized substrates or inhibitory compounds were released from the enzymatic pre-treatment and shows no loss of performance between synthetic and real MSW hydrolysate. We therefore continued this study using synthetic substrates as a proxy for the real MSW hydrolysate.

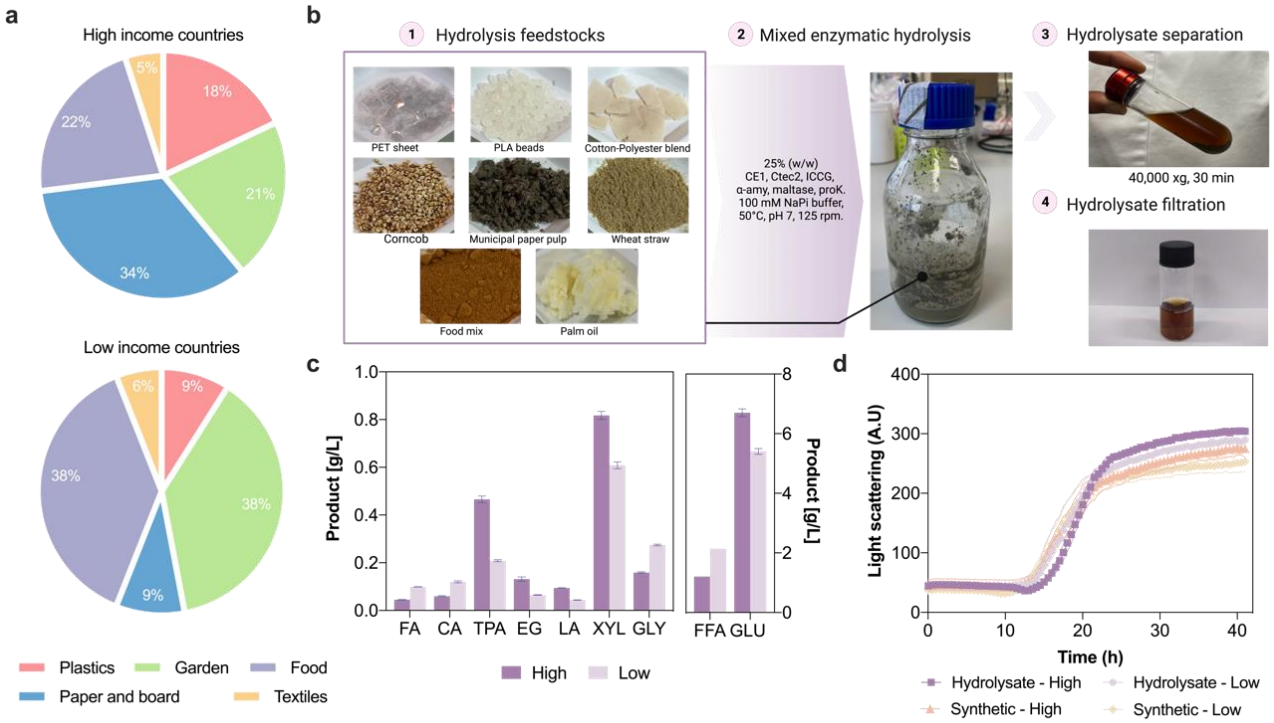

Figure 4. Enzymatic hydrolysis of different MSW representations. (**a**) Adjusted waste composition from high- and upper-middle income countries (up) and lower-middle- and low-income countries (down). (**b**) Photos of the workflow for enzymatic hydrolysis and preparation of hydrolysate from both waste compositions. The selected waste fractions are prepared for hydrolysis (1) before being mixed to the according proportions at a 25% solid loading (w/w) and enzymatically hydrolysed at 50ºC for 72 hours (2). The crude hydrolysates were then separated by centrifugation (3) and filtered (4). (**c**) Enzymatic hydrolysis of both high and low-income waste compositions. (**d**)

Microbioreactor growth assays with tphKAB-XylABE in both real and synthetic waste hydrolysates. All data are means ± SD of N = 3 biological replicates.

Enzymatically processed MSW affords sufficient carbon for efficient RTP and PHA prodcution

To demonstrate a final proof-of-concept of the proposed bioprocess, we assessed the ability of the engineered tphKAB-XylABE strain to produce valuable products, including recombinant therapeutic proteins (RTP) and endogenous produced polyhydroxyalkanoate (PHA), directly from MSW-derived subtrates. Working on the knowledge obtained from the initial section of this work, we investigated production of a human therapeutic protein, IFNα2a, as a high-value illustrative product. For this, we utilised the p131CB10-tphKAB-IFN2a plasmid generated earlier and transformed it into the xylose-catabolizing strain, tphKAB-XylABE. *P. putida* KT2440 natively synthesizes PHAs from acetyl-CoA under nitrogen-limiting conditions[46]. We therefore sought to separately produce PHAs as a low-value illustrative product without any additional engineering. Scale-up flask cell growth assays were set up with both the high and low-income hydrolysates for both products.

Growth and consumption dynamics were similar for both products in each waste composition, and after 60h all biomass-producing substrates were completely depleted (**Fig. 5**). Higher biomass yields were obtained in the low-income cultivations, yielding 0.52 g_{CDW}/g_{SUB} for IFNa2a and 0.56 g_{CDW}/g_{SUB} for the PHA, whereas 0.47 g_{CDW}/g_{SUB} and 0.49 g_{CDW}/g_{SUB} were obtained in the high-income (IFNa2a and PHAs, respectively).

Expression of IFNα2a was successfully observed in both hydrolysates, although to a slightly higher concentration in the low-income hydrolysate (3.9 mg L^{-1} and 5.3 mg L^{-1}, respectively) (**Fig. 5a**). In both waste compositions, RTP production, as well as biomass, reached a maximum titre by about 36 h, even though some carbon was still available. However, protein yield remained stable, and no significant protein degradation was seen after a further 36h, concurring with the onset of ethylene glycol metabolism. Production of PHA was likewise successfully observed in both hydrolysates, reaching maximum yields of 23.06 ± 0.95% and 26.67 ± 0.65%of the cell dry weight (%CDW) after 60 h. The PHAs produced for both mixtures primarily consisted of 3-hydroxydecanoic acid and 3-hydroxydodecanoic acid (**Fig. 5b**). The delayed onset of PHA production compared to RTP production is explained by the slow depletion of available nitrogen and differences in carbon contribution to each product (**Fig. S17**). Together, although the total carbon amount in the low-income hydrolysate was higher, both high- and low-income cultivations efficiently funnelled on average a total of 50% of the available carbon into biomass (including IFNα2a and PHA), reflected by the similar carbon balance profiles obtained for both products (**Fig. 5c-d**). This again suggests that the engineered strain is not only able to convert the available carbon efficiently and consistently into biomass, but this can also translate into desired biomass-associated production. Together, this data demonstrate the efficient conversion of waste hydrolysate into human therapeutic proteins and bioplastic monomers, providing a proof-of-concept for the complete biological upcycling of municipal solid waste into valuable products, regardless of waste composition.

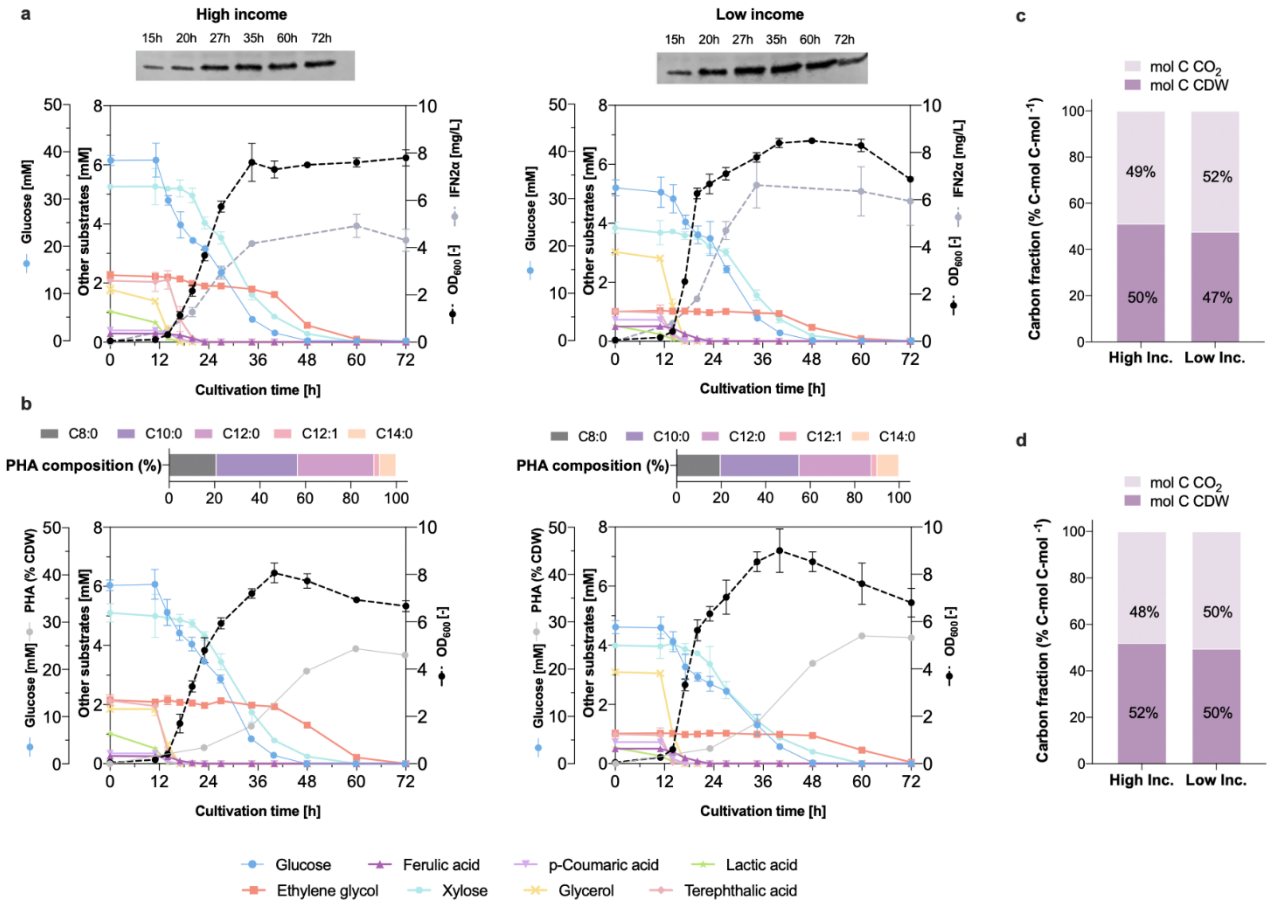

Figure 5. Bioconversion of hydrolysate from municipal solid waste into biotherapeutics and biopolymer. (**a**) Bacterial growth, substrate utilisation and IFNα2a accumulation from tphKAB-XylABE in high- (left) and low-income (right) waste hydrolysates in flask cultivations. Western blots show total cell samples taken at periodic time intervals. (**b**) Bacterial growth, substrate utilisation and PHA accumulation from tphKAB-XylABE in high- (left) and low-income (right) waste hydrolysates in flask cultivations. Shown above are compositions of PHA produced from both hydrolysates. (**c**) Carbon balancing profiles for both IFNα2a producing cultivations. (**d**) Carbon balancing profiles for both PHA-producing cultivations. For **a** and **b,** data points are means ± SDs of N = 3 biological triplicates.

Discussion

The bioprocess concept demonstrated here describes a versatile and fully biological means for the direct conversion of MSW into value-added bioproducts. This process combines enzymatic depolymerisation of the most common carbon-based MSW fractions with direct microbial fermentation and bioconversion of the resulting monomer rich hydrolysates. Biotherapeutic and biopolymer production was validated across two relevant waste composition scenarios pertaining to high- or low-income countries, demonstrating the ability to overcome inherent challenges in MSW valorisation, namely compositional heterogeneity, and variability.

The development of this process relied greatly on the selection and engineering of a robust microbial host for (i) high catabolic diversity, and (ii) flexible and adaptable metabolism, which together allow for efficient co-assimilation and bioconversion of all waste-released carbon. The soil-dwelling *P. putida* KT2440 displays diverse and broad *cis*-metabolism[32], the architecture of which can be readily expanded to incorporate *trans*-catabolism of non-native substrates and product synthesis reactions. Here, we promptly introduced *trans*-metabolism for those MSW derived substrates where no native upstream pathways were present, namely xylose, and the PET plastic monomers TPA and EG. As established, xylose assimilation can be afforded by the incorporation of a *D*-xylose isomerase pathway from *Escherichia coli*[34,43]. Similarly, catabolism of TPA in *P. putida* can be engineered by incorporation of the *tph* operon from *Comamonas* sp. E6[36,37,47], which converts TPA to the central aromatic intermediate PCA that *P. putida* can then natively assimilate. In regards to EG assimilation, most engineering efforts to date have focused on the overexpression of glyoxylate carboligase (*gcl*), which allows for biomass formation via the glycerate pathway[37,41,47,48]. Natively, this pathway is repressed in *P. putida*, and so ethylene glycol funnels directly into the glyoxylate shunt, without leading to biomass formation. This shunting has instead been shown to result in a surplus of reducing equivalents when used as an acetate co-feed[39]. We therefore hypothesized that likewise utilising EG as a co-substrate, with the gluconeogenic substrate TPA, via its native shunt configuration could provide elevated concentrations of reducing equivalents as well as increased flux through amino acid biosynthesis precursors, favourable properties for recombinant therapeutic protein (RTP) production from PET monomers. Our results support this hypothesis, as when grown on both TPA and EG, assimilation of EG via this native configuration provided an enhancement in recombinant protein titres an average of 7-fold over the engineered glycerate pathway configuration. In all, this demonstrates the potential of using EG as a co-substrate derived from waste PET plastic for energy demanding and protein biosynthesis reactions. Moreover, production of therapeutic proteins expands the current range of products that have been derived from PET plastic valorisation[35,48–50].

Due to its metabolic advantages, *P. putida* has been extensively used as a biomanufacturing host to obtain high yields of platform chemicals[32]. While these efforts have enabled bioproduction of numerous valuable products, the carbon substrates used have predominantly comprised of single

carbohydrates such as glucose. This provokes the question as to whether MSW, a complex feedstock, could be suitable for bioproduction from *P. putida*. To determine the answer, the growth and consumption efficiency of the individual substrates derived from MSW was assessed. The most reduced substrates, fatty acids, glycerol, and lactic acid promoted the highest biomass yields, and less than 35% of the carbon from these substrates was lost to CO_2. By comparison, glucose funnelled 46% of carbon to CO_2, while the oxidised aromatics terephthalate and *p*-coumarate resulted in the highest carbon loss to CO_2 (more than 65% of their C-mol)(**Fig. 3a**). These results are consistent with previous modelling studies that predicted that higher product yields are obtained from reduced substrates[51]. This indicates that using feedstocks composed primarily of reduced monomers, such as triglyceride-enriched waste fractions, could result in more sustainable and efficient processes than those currently performed using carbohydrates, like glucose, as a higher proportion of carbon is funnelled into biomass accumulation and product formation as opposed to CO_2 emission. Indeed, glycerol has shown promising results for the cost-efficient and sustainable production of polyhydroxyalkanoate (PHA) in *P. putida* [52,53]. Importantly, we show that this high metabolic efficiency is maintained in a mixed substrate environment, and all monomers were co-metabolised and consumed by the engineered *P. putida*. Strikingly, the individual metabolic efficiencies were also conserved across complex mixtures of all substrates, in conditions ranging between 0.15 and 1.25 of total C-mol. We found that across these sets of treatments, the same proportion of consumed carbon from each substrate was always converted to biomass, alluding to strong prospects for scalability (**Fig. 3e**). Moreover, in the equimolar mixture, no significant lag or diauxic interruption to the growth behaviour between the different substrates was observed (**Fig. 3b**). This can likely be attributed to the reverse carbon catabolite repression (rCCR) mechanism present in *P. putida*, which operates at the mRNA level – contrary to transcriptional CCR in microorganisms like *E. coli* and *B. subtilis*[54–56]. This post-transcriptional regulation has evident physicochemical advantages, which allow for an extremely rapid and sensitive response to substrate availability. In *P. putida,* this mechanism confers a preference for gluconeogenic substrates[33,56,57], although studies have previously demonstrated that in nutritionally complex environments, glycolytic and gluconeogenic co-utilisation can coexist[45,58–60]. In this current work, we showed that lactic acid is preferentially consumed, and C_5 sugars and aromatics were least favoured. However, during mid-exponential growth, all available substrates were co-utilised, displaying active flow in both gluconeogenic and glycolytic directions, in an overall gluconeogenic configuration (**Fig. 3c**). Prior investigation into mixed complex feedstocks has not been extensive, and has not expanded far beyond bioconversion from lignocellulosic biomass and carbohydrate mixtures[61–63]. Previous strategies to allow for substrate co-utilisation have consisted of *crc* elimination[34,35], however this has shown to be detrimental in some instances[44].

In terms of limitations and potential for future development, the product exemplars used here serve only as illustrative high- and low-value products that could be produced using MSW as a

biomanufacturing feedstock, and it is worth noting that further optimisation work will access higher RTP and PHA titres in an effort to reach greater economic viability [46,64–66]. Metabolic engineering and synthetic biology will also bring opportunities to expand the range of usable monomers and achievable end-products. In the quest to establish carbon-neutral circular biorefineries, monomers of polymers that could result in long-term carbon sequestration are advised[67]. Similarly, whilst the enzymatic pre-treatment utilised in this work afforded sufficient carbon for bioproduction, the illustrative feedstocks were limited to only those amenable to enzymatic hydrolysis – with the exclusion of a protein fraction as the required proteinase concentration would compromise the efficacy of the other enzymes within the cocktail. However, as the engineered *P. putida* chassis can directly co-utilise complex substrate mixtures, any hydrolysis reaction that can generate monomers that can be fed into metabolism could be incorporated. For instance, a mixture of non-biodegradable plastics was recently depolymerised by metal-catalysed autoxidation[35], and various alternative pre-treatment methods exist for lignocellulose and plastics, such as chemical hydrolysis, chemical glycolysis or thermolysis[50,62,63,68–73]. Further enzymatic optimisation efforts together with the discovery and engineering of novel enzymatic cocktails – especially those working under mild and mesophilic conditions, will aid the development of sustainable MSW pre-treatment strategies[74]. Generally, as advances in the field of pre-treatment occur, the range of feedstocks that can be incorporated into a MSW-fed bioprocess will likely also be significantly expanded, with other relevant fractions, such as rubber or textiles like leather[17], being viable options. While we did not observe evidence for the accumulation of toxic or harmful compounds originating from the hydrolysis of the selected MSW fractions, true post-consumer waste streams and processes will likely release additives and inhibitors (i.e. dyes, plasticizers) that could interfere with growth[75,76]. However, a number of chemical, biological and physical detoxification strategies are available[77]. Therefore, as our knowledge of the metabolic capabilities in *P. putida,* enzymatic depolymerisation approaches, and process development expands, so will the range of waste streams and products that can be incorporated into the proposed bioprocess.

In summary these results lay a foundation for the bioconversion of complex and variable MSW feedstocks into added value bioproducts. This study serves as a testament to the inherent metabolic versatility and consistency of *P. putida*, and ultimately suggests MSW is a promising biomanufacturing feedstock, regardless of its compositional variability. While current global management efforts are being made to prevent, reduce, and recycle waste, its generation will undoubtedly never be eliminated. In a circular bio-based economy, this unavoidable waste can be utilised as a resource, and maintained for as long as possible in a closed loop. Under this new philosophy, new biomanufacturing and advanced biorefinery approaches will therefore be critical to derive value from waste. This work demonstrates a starting point.

Methods

Plasmid construction

All plasmid construction and sequence details can be found in Tables S1-4. All DNA synthesis and oligonucleotide primer synthesis was performed by Integrated DNA Technologies. The *XylABE* operon was amplified directly from the genome of *E. coli* BL21(DE3). DNA amplification for plasmid construction was performed using Q5 Hot Start High-Fidelity 2x Master Mix (NEB), and colony PCR was performed using Phire Green Hot Start II PCR Master Mix (Thermo Fisher Scientific). Plasmid assembly was performed using NEBuilder HiFi DNA Assembly Master Mix (NEB), followed by transformation into NEB 5-alpha competent *E. coli* cells. To validate correct plasmid assembly, Sanger sequencing was performed (Eurofins Genomic, Germany).

Strain construction

P. putida KT2440 genomic knockout and integration strains were created using the sucrose counter-selection method as described previously[78]. Briefly, electrocompetent cells were transformed with 1µg of the relevant pK18mobsacB-derived plasmid (Supplemental Table 2) and plated on LB+ Kan_{20} and incubated at 30℃. Individual colonies were streaked onto YT+25% sucrose (10 g/L yeast extract, 20 g/L tryptone, 250 g/L sucrose, 18 g/L agar) for counter selection. Individual colonies were selected and streaked once more onto YT+25% sucrose and LB+ Kan_{20} to validate genomic exchange and plasmid loss. Successful modification was further validated by cPCR and Sanger sequencing (Eurofins Genomic, Germany).

Expression and purification of the leaf-branch compost cutinase (LCC) mutant

The LCC (ICCG)[79] gene was expressed in BL21(DE3) cells in a Type NLF 22, 30 L BioEngineering fermenter containing 20 L enhanced 2xYT medium (20 g/L yeast extract, 32 g/L tryptone, 17g/L NaCl, 2 g/L glucose, 17.6 mM Na_2PO_4 (pH 7.4)) at 37°C. Once at an OD_{600} of 0.8 was reached 0.25 mM isopropyl-β-D-1-thiogalactopyranoside (IPTG) was added and the temperature was reduced to 20°C for overnight incubation under a continuous compressed air gas flow of 30 L min^{-1}. Cells were harvested by centrifugation (4 °C, 6000 *g* for 10 minutes) and cell pellets (~100g) were resuspended in buffer A (200 mM NaCl, 50 mM Tris pH 7.5) supplemented with DNase, RNase (Sigma) and Complete EDTA-free protease inhibitor cocktail (Roche). Cells were lysed using a cell disruptor (Constant Systems Ltd.) at 20,000 psi and the lysate was clarified by centrifugation at 125,000 *g* for 90 minutes. The supernatant was applied to a Ni-NTA agarose drip column (Qiagen) and eluted with buffer A supplemented with 250 mM imidazole. Imidazole was removed from the eluted protein using a 10-DG desalting column (Bio-Rad) and purified to homogeneity with a 5 mL HiTrap HP column (GE healthcare) attached to a ÄKTA pure purification system using a linear gradient of 0-250 mM imidazole in buffer A over 35 CV. Fractions were subjected to SDS-PAGE analysis (BioRad, Mini-Protean TGX stain free precast SDS-gel with a 4-20% gradient) and those found to contain the purified protein were pooled and concentrated using a 10 kDa molecular weight cut-off Vivaspin spin column centrifugal concentrator (GE Healthcare) at 3894 x g and 4°C. Imidazole was removed using a 10-DG desalting column (Bio-Rad) and aliquoted, flash frozen in liquid nitrogen and stored at - 80 °C until required.

Mixed waste enzyme hydrolysis

All waste materials and enzymes used are listed in Table S5. Mixed waste hydrolysis was carried out at 25% solid loading (w/w) in 100 mM sodium phosphate buffer pH 7.0 in 500 mL baffled bottles at 50℃ and 125 rpm for 72h. The substrate composition of high- and low-income waste is described in Table S7. Mixed waste slurry was incubated at 50℃ for 1 hour prior to the addition of enzyme: 50 mg CTEC-2/g lignocellulosic substrate, 0.75 mg LCC/g PET substate, 1 mg CE1/g lignocellulosic substrate, 9 U CAL-B/g palm oil, 10 U α-amylase/g starch, 5 U maltase/g starch, and 500 µg/mL carbenicillin were added to the slurry. Separately, 0.5 mg Proteinase K/g PLA substrate and PLA was incubated at 50℃ to promote absorption before addition to the mixed waste slurry. Hydrolysate samples were taken at 8, 24, 48, and 72 hours, crudely filtered, ultracentrifuged at 40,000 g for 30 minutes, and passed through a 0.22 µm filter for fine filtration and sterilisation. Samples were taken for product quantification pre and post 0.22 µm filtration. Hydrolysates were stored at -20℃. Individual substrate hydrolyses were carried out as described above with variable solid loadings (1-10 % w/w) and 0.1% sodium azide (NaN_3) as an antimicrobial agent instead of carbenicillin.

***P. putida* growth and consumption on individual and mixed substrates**

Precultures of wild type and engineered *P. putida* KT2440 were incubated in M9 (6.78 g/L Na_2HPO_4, 3 g/L KH_2PO_4, 0.5 g/L NaCl, 1 g/L NH_4Cl, 2 mM $MgSO_4$, 100 µM $CaCl_2$, 1x trace elements) +/- antibiotic and 5 mM carbon source(s) at 30 ℃ and 180 rpm for 12-24h. Flasks containing 100 mL M9 +/- 500 ug/L carbenicillin and 10 mM of respective carbon source(s) were inoculated in triplicate from the preculture to an OD_{600} of 0.05 and incubated at 30 ℃ and 180 rpm. Intermittent samples were taken to determine OD_{600}, cell dry weight (CDW), and substrate consumption. For the latter, 2 mL of culture was centrifuged at 4000 rpm and 4 ℃ for 10 minutes before the supernatant was filtered through a 0.22 µm filter and stored at -20 ℃. For those cultures in which free fatty acid (C12:0-C18:0) was used as a carbon source, solid substrate precipitation prevented quantification of consumption. To evaluate the free fatty acid consumption rate, linoleic acid (C18:2) – which is an oil at room temperature, was used. M9+ 10 mM linoleic acid was incubated shaking at 180 rpm for 2 hours to create an emulsion prior to inoculation with *P. putida*, and samples were taken while cultures remained shaking. CDW was determined by centrifuging 1 mL of culture at 4000 rpm for 2 minutes in a pre-weighed microcentrifuge tube, followed by discarding the culture supernatant, washing the cell pellet in 1 mL of M9 once, and incubating the cell pellet for 16 h at 50 ℃ before determining the dry pellet weight.

***P. putida* growth, consumption, and production on mock High-Income and Low-Income mixed waste hydrolysate**

P. putida Δ*gcd*::*XylABE* harbouring either tphKAB or tphKAB-IFNα2a was pre-cultured as described above, followed by inoculation in triplicate into 0.9 mL of corresponding hydrolysate and incubated in 48-well flower plates in a BioLector® at 30 ℃ for 48 h (m2p-labs GmbH, Germany). For flasks cultivations, pre-cultures were inoculated in triplicate into 400 mL of M9+ 500 µg/L carbenicillin plus mock high Income hydrolysate (37 mM glucose, 5.4 mM xylose, 2.2 mM TPA, 2.2 mM ethylene glycol, 0.23 mM ferulic acid, 0.37 mM coumaric acid, 1 mM lactic acid, 1.7 mM glycerol, 0.1 mM C12:0, 0.15 mM C14:0, 2.3 mM C16:0, 0.25 mM C18:0, 1.8 mM C18:1; 0.5 mM C18:2) or low Income hydrolysate (30 mM glucose, 4 mM xylose, 1 mM TPA, 1 mM ethylene glycol, 0.5 mM ferulic acid, 0.73 mM coumaric acid, 0.5 mM lactic acid, 3 mM glycerol, 0.18 mM C12:0, 0.27 mM C14:0, 4 mM C16:0, 0.45 mM C18:0, 3.15 mM C18:1; 0.9 mM C18:2) to an OD_{600} of 0.05 and incubated at 30 ℃ and 180 rpm. Intermittent samples were taken to determine OD_{600}, CDW, substrate consumption and

product formation as described above, with the following exceptions: (i) no free fatty acid quantification was performed at they initially formed a solid precipitate, (ii) at intermittent time points 5 mL of culture pellet was harvested and stored at -20 ℃ for product quantification.

Analytics

Quantification of Glucose, Xylose, Glycerol and Lactic acid by HPLC

All chemicals and reagents are listed in Table S5. 5 µL of neat 0.22 µm filtered culture supernatant or enzyme hydrolysate containing monomeric sugar (D-glucose and D-xylose), glycerol and/or L-lactic acid was injected and separated by a Supelcogel™ C–610H (6% Crosslinked) column operating at 30 ℃ with an isocratic 0.1% (v/v) H_3PO_4 mobile phase run at a flow rate of 0.5 mL/min. Sugars and glycerol were quantified from the RID, and lactic acid was quantified from the UV at 210 nm. Product identification and quantification was carried out using authentic standards.

Quantification of TPA, Ferulic acid, Coumaric acid, and relevant metabolic acid intermediates by HPLC

300 µL of 0.22 µm filtered culture supernatant or enzyme hydrolysate was appropriately diluted and combined with 300 µl methanol and 13 µl of 3M HCl prior to injection of 10 µL onto a Agilent 1200 Infinity Series HPLC with a Kinetex 5 µm C18 100 Å column, 250 x 4.6 mM column (Phenomenex®) operating at 25 ℃ with a flow rate of 0.8 mL/min and a linear gradient of 5% acetonitrile:95% H_2O to 30% acetonitrile:70% H_2O over 20 minutes with a 4 minutes post run hold at 5% acetonitrile:95% H_2O. All solvent contained 0.1 % TFA. All acids were quantified from the UV at 260 nm. Product identification and quantification was carried out using authentic standards

Quantification of Ethylene glycol by HPLC

300 µL of 0.22 µm filtered culture supernatant or enzyme hydrolysate was appropriately diluted and combined with 350 µL of 40% NaOH (w/v) and mixed thoroughly before the addition of 10 µL benzoyl chloride and incubation at 40 ℃ and 4000 rpm for 20 minutes. Samples were extracted into 1 mL of hexane, of which 500 µL was put into a 1.5 mL glass vial and dried fully under nitrogen before resuspension in 1 mL of H_2O. 10 µL of derivatized sample was injected onto a Agilent 1200 Infinity Series HPLC with a Kinetex 5 µm C18 100 Å column, 250 x 4.6 mM column (Phenomenex®) operating at 25 ℃ with an isocratic 55% acetonitrile (0.1% TFA): 45% H_2O (0.1% TFA) mobile phase at a flow rate of 1 mL/min. Derivatized ethylene glycol was quantified from the UV at 230 nm. Product identification and quantification was carried out using authentic standards

Quantification of free fatty acid by GC-MS

500 µL of 0.22 µm filtered culture supernatant or enzyme hydrolysate spiked with 10 µg of pentadecanoic acid (C15:0) as an internal standard before being extracted with 1 mL of 2:1 chloroform/toluene. The organic phase was washed with 1 mL of 0.9% NaCl (w/v) before being dried down under nitrogen gas. Dried sample was resuspended in 3 mL of 1 M MeOH-HCl and incubated at 50 ℃ for 60 minutes in a sealed vessel. Once cooled to room temperature, 0.9% NaCl (w/v) was added before extraction with a variable volume of hexane. Fatty acid methyl esters (FAMEs) were quantified using an Agilent Technologies 5975 MSD coupled to a 7890B GC with a PAL RSI 85 autosampler and an Agilent VT-5HP column (30 m x 0.25 mM x 0.1 µM). Injector temperature was set to 240 ℃ with a split ratio of 1:100 (1 µL injection). Column temperature was held at 140 ℃ for 5 minutes before ramping at 10 ℃/min to 300 ℃ and being held for 7 min. Ion source temperature of the mass spectrometer (MS) was set to 230 ℃ and spectra were recorded from m/z 50 to m/z 550. Compound identification was carried out using authentic standards and comparison to the reference spectra in the NIST library.

Quantification of PHA monomers by GC-MS

At discrete timepoints during the time course of PHA production by a relevant strain of *P. putida*, 2 mL of culture was centrifuged at 4000 rpm for 10 minutes at 4 ℃, the culture supernatant was discarded, and the cell pellet was washed twice in 5 mL of 0.9% NaCl (w/v) before being lyophilized. Methanolysis was then carried out by resuspending the lyophilized cell pellet in 3 mL of 1 M MeOH-HCl with 25 µg of benzoic acid as an internal standard and incubating at 100 ℃ for 150 min in a sealed vessel. Once cooled to room temperature, samples were washed with 0.9% NaCl (w/v) before being extracted with 2 mL of hexane. Quantification of hydroxyacid methyl esters (HAMEs) was carried out by GC-MS as described in the section above with the following exceptions: split ratio of 1:10, column temperature was initially held at 50 ℃ or 5 minutes before ramping at 10 ℃/min to 280 ℃ at being held for 5 min. Compound identification was carried out using authentic standards and comparison to reference spectra in the NIST library.

Western blot and quantification of heterologous IFNα2 production

At either a final time point or discrete timepoints throughout a growth course with the relevant strain of *P. putida*, 5 mL of culture was harvested, centrifuged, and the cell pellet was resuspended in lysing buffer (1µL benzonase nuclease, 1 tablet protease inhibitor cocktail in 50ml 1xPBS) before sonication. Samples for comparison of protein production by *P. putida* tphKAB to strain tphKAB-EG12 were resuspended to an according volume for normalisation to OD_{600} = 10. Samples for IFNα2a quantification were resuspended to a normalising volume to OD_{600} = 20. Sonicated samples were resuspended in SDS-PAGE loading buffer (ThermoFisher), supplemented with 75mM dithiothreitol and heated at 95 ℃ for 10 minutes. Equal amounts of whole cell protein were separated on a 15% SDS-polyacrylamide gel (Bio-Rad) by SDS-PAGE. The SDS gel was then transferred to a nitrocellulose membrane and blocked with 5% skimmed milk in PBS. Membranes were incubated overnight (50 rpm, 4°C) with either mouse anti-His monoclonal (Thermo Fisher; 1:3000 in 5% skimmed milk) or anti-IFNa2 primary antibody (abcam, 193055, 1:2000 in 5% skimmed milk). Membranes were washed with PBS, followed by incubation with an IRDye anti-mouse or anti-rabbit IgG secondary antibody (LI-COR; 1:30000 in 5% skimmed milk). IFNα2a samples were quantified based on densitometry analysis using Li-Cor Image Studio 5.0 against pure IFNα2a protein standards of known concentrations prepared in the same way.

Data analyses, model construction, and simulation

The most recent genome-scale metabolic model of *P. putida* KT2440, iJN1463[80] was extended to incorporate modifications for TPA and xylose metabolism. For EG, the glyoxylate carboligase reaction, GLXCL, was eliminated to simulate operon repression. The final model was subjected to flux balance analysis (FBA) using the COBRA toolbox [81] with the linear programming solver Gurobi (www.gurobi.com) in MATLAB 2020a (Mathworks Inc.). To predict flux variation from the equimolar experiment, the model was constrained with uptake rates obtained experimentally and the biomass reaction was set as the objective function. ATP maintenance requirements were fixed at 0.92 mmol $gCDW^{-1}$ h^{-1}. A prediction of the total CO_2 produced was calculated by multiplying the resulting CO_2 production rate against the total growth time for the specified period. Statistical significance or correlation analysis were performed by with Prism 9 (GraphPad Software, Inc). All experiments were performed in at least three biological triplicates. Manual linear regression analysis was performed during exponential growth phase to calculate growth rate (µ) and specific uptake rate on the

corresponding substrate(s) (q_s). The biomass yield when using mixed substrates ($Y_{S/X}$) was calculated as a lumped value. The total amount of carbon (C-mol) for biomass was based on the elemental carbon composition of *P. putida* KT2440[82], calculated to be 24.5 g/mol.

Authors' contributions

GAG, MC, AB, KF, planned and performed the experiments. GAG, MC, and ND analysed the data and wrote the manuscript. All authors read and approved the final version of the manuscript.

Availability of data and materials

All data generated or analysed in this study are included in this manuscript or in supplemental material.

Competing interests

The authors disclose no conflicts.

Funding

GAG is support by a BBSRC DTP grant (BB/M011208/1). MC and AB were supported by BBSRC Responsive mode grant (BB/P01738X/1).

Acknowledgements

We would like to acknowledge Rehana Sung and the MIB separation facility, Ross Kent for supporting early catabolic constructs assembly efforts, and Joseph Webb for supporting with fermentation.

References

1. United Nations. The sustainable development goals report 2022. *United Nations Publ. issued by Dep. Econ. Soc. Aff.* 68 (2022).

2. Friedlingstein, P. *et al.* Global Carbon Budget 2021. *Earth Syst. Sci. Data* **14**, 1917–2005 (2022).

3. WEF. *The Global Risks Report 2023 18th Edition*. *World Economic Forum* www.weforum.org (2023).

4. UNFCC. *Adoption of the Paris Agreement*. *Conference of the Parties on its twenty-first session* vol. 21932 http://unfccc.int/resource/docs/2015/cop21/eng/l09r01.pdf (2015).

5. Intergovernmental Panel on Climate Change. Climate Change 2022 - Mitigation of Climate Change - Full Report. *Cambridge Univ. Press* 1–30 (2022).

6. Culaba, A. B. *et al.* Design of biorefineries towards carbon neutrality: A critical review. *Bioresour. Technol.* **369**, 128256 (2022).

7. Calvo-Flores, F. G. & Martin-Martinez, F. J. Biorefineries: Achievements and challenges for a bio-based economy. *Front. Chem.* **10**, 1329 (2022).

8. Mohr, A. & Raman, S. Lessons from first generation biofuels and implications for the sustainability appraisal of second generation biofuels. *Effic. Sustain. Biofuel Prod. Environ. Land-Use Res.* **63**, 281–310 (2015).

9. Magnan, A. K. *et al.* Sea level rise risks and societal adaptation benefits in low-lying coastal areas. *Sci. Rep.* **12**, 1–22 (2022).

10. Kulp, S. A. & Strauss, B. H. New elevation data triple estimates of global vulnerability to sea-level rise and coastal flooding. *Nat. Commun.* **10**, 1–12 (2019).

11. Zambare, V. P. & Christopher, L. P. Integrated biorefinery approach to utilization of pulp and paper mill sludge for value-added products. *J. Clean. Prod.* **274**, 122791 (2020).

12. Gaspar, M. C. *et al.* Assessment of Agroforestry Residues: Their Potential within the Biorefinery Context. *ACS Sustain. Chem. Eng.* **7**, 17154–17165 (2019).

13. Teigiserova, D. A., Hamelin, L. & Thomsen, M. Review of high-value food waste and food residues biorefineries with focus on unavoidable wastes from processing. *Resour. Conserv. Recycl.* **149**, 413–426 (2019).

14. Kaparaju, P., Serrano, M., Thomsen, A. B., Kongjan, P. & Angelidaki, I. Bioethanol, biohydrogen and biogas production from wheat straw in a biorefinery concept. *Bioresour. Technol.* **100**, 2562–2568 (2009).

15. Venkata Mohan, S., Dahiya, S., Amulya, K., Katakojwala, R. & Vanitha, T. K. Can circular bioeconomy be fueled by waste biorefineries — A closer look. *Bioresour. Technol. Reports* **7**, 100277 (2019).

16. Vinti, G. *et al.* Municipal Solid Waste Management and Adverse Health Outcomes: A Systematic Review. *Int. J. Environ. Res. Public Health* **18**, (2021).

17. Kaza, S., Yao, L. C., Bhada-Tata, P. & Van Woerden, F. *What a Waste 2.0: A Global Snapshot of Solid Waste Management to 2050*. *World Bank Publications* (2018) doi:10.1596/978-1-4648-1329-0.

18. Nizami, A. S. *et al.* Waste biorefineries: Enabling circular economies in developing countries. *Bioresour. Technol.* **241**, 1101–1117 (2017).

19. Abbasi, S. A. The myth and the reality of energy recovery from municipal solid waste. *Energy. Sustain. Soc.* **8**, 1–15 (2018).

20. Vergara, S. E. & Tchobanoglous, G. Municipal solid waste and the environment: A global perspective. *Annu. Rev. Environ. Resour.* **37**, 277–309 (2012).

21. Son, J. *et al.* Customized valorization of waste streams by Pseudomonas putida: State-of-the-art, challenges, and future trends. *Bioresour. Technol.* **371**, 128607 (2023).

22. Pérez, V. *et al.* Integrated innovative biorefinery for the transformation of municipal solid waste into biobased products. in *Waste Biorefinery: Integrating Biorefineries for Waste Valorisation* 41–80 (2020). doi:10.1016/B978-0-12-818228-4.00002-2.

23. Blazek, J. & Gilbert, E. P. Effect of enzymatic hydrolysis on native starch granule structure. *Biomacromolecules* **11**, 3275–3289 (2010).

24. Van Dyk, J. S. & Pletschke, B. I. A review of lignocellulose bioconversion using enzymatic hydrolysis and synergistic cooperation between enzymes-Factors affecting enzymes, conversion and synergy. *Biotechnol. Adv.* **30**, 1458–1480 (2012).

25. Chandra, P., Enespa, Singh, R. & Arora, P. K. Microbial lipases and their industrial applications: A comprehensive review. *Microb. Cell Fact.* **19**, 1–42 (2020).

26. Mora, L. & Toldrá, F. Advanced enzymatic hydrolysis of food proteins for the production of bioactive peptides. *Curr. Opin. Food Sci.* **49**, 100973 (2023).

27. Pleissner, D. & Lin, C. S. K. Valorisation of food waste in biotechnological processes. *Sustain. Chem. Process.* **1**, 1–6 (2013).

28. Iqbal, H. M. N., Kyazze, G. & Keshavarz, T. Advances in the valorization of lignocellulosic materials by biotechnology: An overview. *BioResources* **8**, 3157–3176 (2013).

29. Liu, N., Santala, S. & Stephanopoulos, G. Mixed carbon substrates: a necessary nuisance or a missed opportunity? *Curr. Opin. Biotechnol.* **62**, 15–21 (2020).

30. Wu, Y., Shen, X., Yuan, Q. & Yan, Y. Metabolic engineering strategies for co-utilization of carbon sources in microbes. *Bioengineering* **3**, (2016).

31. Weimer, A., Kohlstedt, M., Volke, D. C., Nikel, P. I. & Wittmann, C. Industrial biotechnology of Pseudomonas putida: advances and prospects. *Appl. Microbiol. Biotechnol.* **104**, 7745–7766 (2020).

32. Nikel, P. I. & de Lorenzo, V. Pseudomonas putida as a functional chassis for industrial biocatalysis: From native biochemistry to trans-metabolism. *Metab. Eng.* **50**, 142–155 (2018).

33. Schink, S. J. *et al.* Glycolysis/gluconeogenesis specialization in microbes is driven by biochemical constraints of flux sensing. *Mol. Syst. Biol.* **18**, 10704 (2022).

34. Elmore, J. R. *et al.* Engineered Pseudomonas putida simultaneously catabolizes five major components of corn stover lignocellulose: Glucose, xylose, arabinose, p-coumaric acid, and acetic acid. *Metab. Eng.* **62**, 62–71 (2020).

35. Sullivan, K. P. *et al.* Mixed plastics waste valorization through tandem chemical oxidation and biological funneling. *Science (80-.).* **378**, (2022).

36. Sasoh, M. *et al.* Characterization of the terephthalate degradation genes of Comamonas sp. strain E6. *Appl. Environ. Microbiol.* **72**, 1825–1832 (2006).

37. Werner, A. Z. *et al.* Tandem chemical deconstruction and biological upcycling of poly(ethylene terephthalate) to β-ketoadipic acid by Pseudomonas putida KT2440. *Metab. Eng.* **67**, 250–261 (2021).

38. Berepiki, A., Kent, R., MacHado, L. F. M. & Dixon, N. Development of High-Performance Whole Cell Biosensors Aided by Statistical Modeling. *ACS Synth. Biol.* **2020**, 36 (2020).

39. Li, W. J. *et al.* Laboratory evolution reveals the metabolic and regulatory basis of ethylene glycol metabolism by Pseudomonas putida KT2440. *Environ. Microbiol.* **21**, 3669–3682 (2019).

40. Wirth, N. T. *et al.* A synthetic C2 auxotroph of Pseudomonas putida for evolutionary engineering of alternative sugar catabolic routes. *Metab. Eng.* **74**, 83–97 (2022).

41. Franden, M. A. *et al.* Engineering Pseudomonas putida KT2440 for efficient ethylene glycol utilization. *Metab. Eng.* **48**, 197–207 (2018).

42. Mikiewicz, D. *et al.* Soluble insulin analogs combining rapid- and long-acting hypoglycemic properties ± from an efficient E. coli expression system to a pharmaceutical formulation.

PLoS One **12**, e0172600 (2017).

43. Dvořák, P. & de Lorenzo, V. Refactoring the upper sugar metabolism of Pseudomonas putida for co-utilization of cellobiose, xylose, and glucose. *Metab. Eng.* **48**, 94–108 (2018).

44. Molina, L., Rosa, R. La, Nogales, J. & Rojo, F. Pseudomonas putida KT2440 metabolism undergoes sequential modifications during exponential growth in a complete medium as compounds are gradually consumed. *Environ. Microbiol.* **21**, 2375–2390 (2019).

45. Kukurugya, M. A. *et al.* Multi-omics analysis unravels a segregated metabolic flux network that tunes co-utilization of sugar and aromatic carbons in Pseudomonas putida. *J. Biol. Chem.* **294**, 8464–8479 (2019).

46. Mezzina, M. P., Manoli, M. T., Prieto, M. A. & Nikel, P. I. Engineering Native and Synthetic Pathways in Pseudomonas putida for the Production of Tailored Polyhydroxyalkanoates. *Biotechnol. J.* **16**, (2021).

47. Brandenberg, O. F., Schubert, O. T. & Kruglyak, L. Towards synthetic PETtrophy: Engineering Pseudomonas putida for concurrent polyethylene terephthalate (PET) monomer metabolism and PET hydrolase expression. *Microb. Cell Fact.* **21**, 1–31 (2022).

48. Tiso, T. *et al.* Towards bio-upcycling of polyethylene terephthalate. *Metab. Eng.* **66**, 167–178 (2021).

49. Sadler, J. C. & Wallace, S. Microbial synthesis of vanillin from waste poly(ethylene terephthalate). *Green Chem.* **23**, 4665–4672 (2021).

50. Diao, J., Hu, Y., Tian, Y., Carr, R. & Moon, T. S. Upcycling of poly(ethylene terephthalate) to produce high-value bio-products. *Cell Rep.* **42**, 111908 (2023).

51. Tiso, T. *et al.* The metabolic potential of plastics as biotechnological carbon sources – Review and targets for the future. *Metab. Eng.* **71**, 77–98 (2022).

52. Beckers, V., Poblete-Castro, I., Tomasch, J. & Wittmann, C. Integrated analysis of gene expression and metabolic fluxes in PHA-producing Pseudomonas putida grown on glycerol. *Microb. Cell Fact.* **15**, 1–18 (2016).

53. Prieto, A. *et al.* A holistic view of polyhydroxyalkanoate metabolism in Pseudomonas putida. *Environ. Microbiol.* **18**, 341–357 (2016).

54. Lv, F. *et al.* Regulation of hierarchical carbon substrate utilization, nitrogen fixation, and root colonization by the Hfq/Crc/CrcZY genes in Pseudomonas stutzeri. *iScience* **25**, 105663 (2022).

55. Green, J. *et al.* Cyclic-AMP and bacterial cyclic-AMP receptor proteins revisited: adaptation for different ecological niches. *Curr. Opin. Microbiol.* **18**, 1–7 (2014).

56. Park, H., McGill, S. L., Arnold, A. D. & Carlson, R. P. Pseudomonad reverse carbon catabolite repression, interspecies metabolite exchange, and consortial division of labor. *Cell. Mol. Life Sci. 2019 773* **77**, 395–413 (2019).

57. Wilkes, R. A., Waldbauer, J. & Aristilde, L. Analogous Metabolic Decoupling in Pseudomonas putida and Comamonas testosteroni Implies Energetic Bypass to Facilitate Gluconeogenic Growth. *MBio* **12**, (2021).

58. Perrin, E. *et al.* Diauxie and co-utilization of carbon sources can coexist during bacterial growth in nutritionally complex environments. *Nat. Commun.* **11**, 1–16 (2020).

59. La Rosa, R., Nogales, J. & Rojo, F. The Crc/CrcZ-CrcY global regulatory system helps the integration of gluconeogenic and glycolytic metabolism in Pseudomonas putida. *Environ. Microbiol.* **17**, 3362–3378 (2015).

60. Wilkes, R. A. *et al.* Complex regulation in a Comamonas platform for diverse aromatic carbon metabolism. *Nat. Chem. Biol.* 1–12 (2023) doi:10.1038/S41589-022-01237-7.

61. Ragauskas, A. J. *et al.* Lignin valorization: improving lignin processing in the biorefinery. *Science (80-.).* **344**, 1246843–1246843 (2014).

62. Linger, J. G. *et al.* Lignin valorization through integrated biological funneling and chemical catalysis. *Proc. Natl. Acad. Sci.* **111**, 12013–12018 (2014).

63. Borchert, A. J., Henson, W. R. & Beckham, G. T. Challenges and opportunities in biological funneling of heterogeneous and toxic substrates beyond lignin. *Curr. Opin. Biotechnol.* **73**, 1–13 (2022).

64. Meyers, A., Furtmann, C., Gesing, K., Tozakidis, I. E. P. & Jose, J. Cell density-dependent auto-inducible promoters for expression of recombinant proteins in Pseudomonas putida. *Microb. Biotechnol.* **12**, 1003–1013 (2019).

65. Liang, T. *et al.* Construction of T7-Like Expression System in Pseudomonas putida KT2440 to Enhance the Heterologous Expression Level. *Front. Chem.* **9**, 556 (2021).

66. Lieder, S., Nikel, P. I., de Lorenzo, V. & Takors, R. Genome reduction boosts heterologous gene expression in Pseudomonas putida. *Microb. Cell Fact.* **14**, 1–14 (2015).

67. Scown, C. D. Prospects for carbon-negative biomanufacturing. *Trends Biotechnol.* **40**, 1415–1424 (2022).

68. Ragaert, K., Delva, L. & Van Geem, K. Mechanical and chemical recycling of solid plastic waste. *Waste Management* vol. 69 24–58 (2017).

69. Vora, N. *et al.* Leveling the cost and carbon footprint of circular polymers that are chemically recycled to monomer. *Sci. Adv.* **7**, (2021).

70. Arnold, S., Moss, K., Henkel, M. & Hausmann, R. Biotechnological Perspectives of Pyrolysis Oil for a Bio-Based Economy. *Trends Biotechnol.* **35**, 925–936 (2017).

71. Zakzeski, J., Bruijnincx, P. C. A., Jongerius, A. L. & Weckhuysen, B. M. The catalytic valorization of lignin for the production of renewable chemicals. *Chem. Rev.* **110**, 3552–3599 (2010).

72. Xu, C., Nasrollahzadeh, M., Selva, M., Issaabadi, Z. & Luque, R. Waste-to-wealth: biowaste valorization into valuable bio(nano)materials. *Chem. Soc. Rev.* **48**, 4791–4822 (2019).

73. Bhatt, M. *et al.* Valorization of solid waste using advanced thermo-chemical process: A review. *J. Environ. Chem. Eng.* **9**, 105434 (2021).

74. Chen, C. C., Dai, L., Ma, L. & Guo, R. T. Enzymatic degradation of plant biomass and synthetic polymers. *Nat. Rev. Chem.* **4**, 114–126 (2020).

75. Rao, P. & Rathod, V. Valorization of Food and Agricultural Waste: A Step towards Greener Future. *Chem. Rec.* **19**, 1858–1871 (2019).

76. Ügdüler, S., Van Geem, K. M., Roosen, M., Delbeke, E. I. P. & De Meester, S. Challenges and opportunities of solvent-based additive extraction methods for plastic recycling. *Waste Manag.* **104**, 148–182 (2020).

77. Jönsson, L. J., Alriksson, B. & Nilvebrant, N. O. Bioconversion of lignocellulose: Inhibitors and detoxification. *Biotechnol. Biofuels* **6**, 1–10 (2013).

78. Marx, C. J. Development of a broad-host-range sacB-based vector for unmarked allelic exchange. *BMC Res. Notes* **1**, 1–8 (2008).

79. Tournier, V. *et al.* An engineered PET depolymerase to break down and recycle plastic bottles. *Nature* **580**, 216–219 (2020).

80. Nogales, J. *et al.* High-quality genome-scale metabolic modelling of Pseudomonas putida highlights its broad metabolic capabilities. *Environ. Microbiol.* **22**, 255–269 (2020).

81. Heirendt, L. *et al.* Creation and analysis of biochemical constraint-based models using the COBRA Toolbox v.3.0. *Nat. Protoc.* **14**, 639–702 (2019).

82. van Duuren, J. B. J. H. *et al.* Reconciling in vivo and in silico key biological parameters of Pseudomonas putida KT2440 during growth on glucose under carbon-limited condition. *BMC Biotechnol.* **13**, 1–13 (2013).